

Article

Catalytic Ozonation of Atrazine Enhanced by Mesoporous CeO₂: Morphology, Performance and Intermediates

Jianlin Zhang ^{1,2} , Tao Zhuang ², Shanjun Liu ², Shan Sun ², Yongxin Wang ², Xinyu Liu ³, Jin Wang ⁴ and Rutao Liu ^{1,*} 

¹ School of Environmental Science and Engineering, China-America CRC for Environment & Health, Shandong University, Qingdao 266000, China

² Jinan Environmental Research Academy, Jinan 250000, China

³ Shandong CRRC Huateng Environment Co. Ltd., Jinan 250000, China

⁴ School of Civil Engineering, Beijing Jiaotong University, Beijing 100000, China

* Correspondence: rutaoliu@sdu.edu.cn

Abstract: Heterogeneous catalytic ozonation is an alternative approach for the removal of refractory pollutants from water, and the fabrication of mesoporous materials with high dispersibility would enhance the catalytic efficiency. A mesoporous CeO₂ was prepared by the nanocasting method with SBA-15 as a hard template, and was investigated in the catalytic ozonation of atrazine. The synthetical CeO₂ nanorods have a specific surface area of 95.08 m²/g, a diameter of 10.16 nm, and a spacing of 2.18 nm. The removal rate of atrazine was 85.5%, 64.8%, and 46.4% in the order of catalytic ozonation by synthetical CeO₂ > single ozonation > catalytic ozonation by commercial CeO₂, respectively. The superior activity of the synthetical CeO₂ could be attributed to the well-ordered mesoporous structure, the high surface area, and the redox Ce³⁺/Ce⁴⁺ cycling. Moreover, eight organic intermediates were identified after one minute of catalytic ozonation of atrazine, and the cleavage of the ethylamino group was proposed as the main pathway of atrazine degradation.

Keywords: catalytic ozonation; atrazine; CeO₂; mesoporous



Citation: Zhang, J.; Zhuang, T.; Liu, S.; Sun, S.; Wang, Y.; Liu, X.; Wang, J.; Liu, R. Catalytic Ozonation of Atrazine Enhanced by Mesoporous CeO₂: Morphology, Performance and Intermediates. *Water* **2022**, *14*, 3431. <https://doi.org/10.3390/w14213431>

Academic Editors: Huijiao Wang, Dionysios (Dion) Demetriou, Dionysiou and Yujue Wang

Received: 29 September 2022

Accepted: 25 October 2022

Published: 28 October 2022

Publisher's Note: MDPI stays neutral with regard to jurisdictional claims in published maps and institutional affiliations.



Copyright: © 2022 by the authors. Licensee MDPI, Basel, Switzerland. This article is an open access article distributed under the terms and conditions of the Creative Commons Attribution (CC BY) license (<https://creativecommons.org/licenses/by/4.0/>).

1. Introduction

Atrazine as a chlorinated triazine herbicide has been widely used in agriculture, especially for the control of crops and grassy weeds [1]. It has a water solubility of 33 mg L⁻¹ at 25 °C, an organic carbon partition coefficient value of 100 L kg⁻¹, and a half-life ranging from 21 days to two years, which makes it possible to leach into the aquatic ecosystem and persist for a long time [2]. Atrazine, even at low concentrations in water bodies, could cause serious negative effects on human health through the accumulation of it in the food chain [3], and has been listed as a priority substance by the European Commission. Notably, the detected concentration of atrazine in surface water and groundwater in Beijing ranged from 0.12 to 5.16 µg L⁻¹, which exceeded the allowable level of 3 µg L⁻¹ for drinking water [4]. However, the traditional water purification methods are obviously not enough to remove atrazine from water efficiently and completely [5], and the by-products such as halogens might cause a more serious ecological impact [6]. Therefore, it is an urgent requirement to develop an effective removal method for reducing its environmental exposure.

Besides persulfate oxidation [7], photocatalytic oxidation [8], and electrochemical oxidation [9], heterogeneous catalytic ozonation technology is a promising technology for the removal of refractory pollutants [10], which could generate highly reactive hydroxyl radicals with a redox potential of 2.80 eV and rapidly and non-selectively degrade or even mineralize antibiotics with 10⁶–10¹⁰ L mol⁻¹ s⁻¹ reaction rate [11]. Li et al. [12] evaluated the degradation of atrazine by the catalytic ozonation of iron scraps, and the results showed that the mineralization efficiency was as high as 86.6%, and the toxicity was efficiently

removed at 30 min. Ye et al. [13] identified that the prepared catalyst could effectively improve the degradation and mineralization rate of atrazine, and the mineralization strongly depended on the solution's pH. Zeghioud et al. [14] concluded that catalytic ozonation coupled with discharge plasma could improve the removal efficiency of refractory organic pollutants. He et al. [15] combined membrane filtration and catalytic ozonation for the removal of atrazine, 99.99% of atrazine could be removed within 40 min and hydroxyl radicals were inferred to be the main reactive oxygen species in the catalytic ozonation process. Three pollutant degradation pathways are normally proposed in the process of heterogeneous catalytic ozonation [16]. Firstly, ozone is adsorbed on the catalyst surface and catalyzed to generate radical oxygen species, which further degrades the organic pollutant adsorbed on the catalyst surface or in solution. Secondly, ozone directly attacks and degrades the organic pollutants adsorbed on the surface of the catalyst or the complex formed by organic pollutants and the catalyst. Thirdly, both ozone and organic pollutants are simultaneously adsorbed and reacted on the surface of the catalyst. Obviously, heterogeneous catalytic processes are really complicated, involving gas phase (ozone), liquid phase (water) and solid phase (catalyst), where catalysts would perform various roles, such as providing active sites for adsorption and catalytic ozonation. Therefore, the textural properties of catalysts, such as surface area, pore volume and porosity, are the keys to catalytic efficiency.

Numerous studies have been devoted to designing and optimizing the properties of catalysts to improve the efficiency of catalytic ozonation. Bing et al. [17] prepared $\text{Fe}_2\text{O}_3/\text{Al}_2\text{O}_3@\text{SBA-15}$ by wet impregnation and calcination, and characterized that Al_2O_3 and Fe_2O_3 were highly dispersed on SBA-15, and amounts of surface Lewis acid sites existed due to the substitution of Al^{3+} for the hydrogen of Si-OH. Yuan et al. [18] synthesized microporous iron silicate with poor crystallinity and found that Fe-Si binary oxides inhibited the futile decomposition of ozone and increased the probability of hydroxyl radicals generated through the reaction between ozone and $\alpha\text{-Fe}_2\text{O}_3$. Our previous work prepared a mesoporous MnO_2 by the nanocasting method and found that the ordered nanorods with a high surface area facilitated mass transport and exposure of active sites [19]. Besides MnO_2 , CeO_2 is another widely studied heterogeneous catalyst for catalytic ozonation. The cerium redox pair (Ce(III) and Ce(IV)) performs a synergetic effect on catalytic ozonation, where Ce(III) could catalyze ozonolysis to generate hydroxyl radicals and would be regenerated through the reduction of Ce(IV) [20]. Notably, the surface basicity, defect density/oxygen vacancies and unsaturated coordination sites of CeO_2 crystal planes exposed are important factors in the catalytic performance, such as the ability of different crystal planes in the order of $(100 + 110) > (100) > (111)$ to enhance the mineralization of nitrophenol [21].

In this study, an ordered mesoporous CeO_2 with a high surface area was prepared with SBA-15 as the hard template by the nanocasting method and used as an efficient catalyst for catalytic ozonation of atrazine. The textural properties of the synthesized samples were characterized by X-ray diffraction (XRD), surface area analysis techniques, scanning electron microscope (SEM), transmission electron microscope (TEM), and X-ray photoelectron spectroscopy (XPS). The performance of CeO_2 was investigated by evaluating the degradation of atrazine under various conditions compared with control samples. Moreover, the degradation pathways were assessed through the identification of intermediate products. This study may provide an approach to effectively remove refractory pollutants in the process of wastewater treatment.

2. Materials and Methods

2.1. Materials

SBA-15 was purchased from XFNANO Co., Ltd. (Nanjing, China). The commercial CeO_2 and $\text{Ce}(\text{NO}_3)_3 \cdot 6\text{H}_2\text{O}$ were supplied by Sinoparm Chemical Reagent Co., Ltd. (Shanghai, China). Atrazine was provided by the laboratory of the government chemist (Germany). NaOH was purchased from Rhawn Reagent (Shanghai, China). H_2SO_4 was obtained from Yantai Far East Fine Chemical Co., Ltd. (Yantai, China). All chemicals

used were of analytical grade without further purification. Deionized water (18 MΩcm) produced by the Milli-Q purification system (Millipore, USA) was used to prepare solutions. Ozone was supplied by an ozone generator (COM-AD-01, ANSEROS), and the ozone stock solution was obtained by bubbling gaseous ozone into a 1 L cylindrical reactor filled with pure water for 30 min.

2.2. Preparation of CeO₂

The synthesis of mesoporous CeO₂ was based on a previously reported method [19]. Concisely, 4.51 g of SBA-15 was dispersed in an ethanol solution (15 mL of ultrapure water and 90 mL of ethanol) under stirring with a magnetic bar at room temperature. A total of 13 g of Ce(NO₃)₃•6H₂O was added into the suspended solution and kept stirring for 2 h. The solid was filtered from the suspension, dried for 5 h at 105 °C, and subsequently calcined at 300 °C for 3 h. The CeO₂/SBA-15 complex obtained was rinsed with 2M NaOH, then washed to neutral with ultrapure water and dried for 3 h at 105 °C.

2.3. Experimental Procedure

The experimental procedure was conducted in batch mode in a 0.6 L cylindrical reactor with a diameter of 80 mm and a height of 120 mm at room temperature. Basically, appropriate amounts of catalyst and atrazine stock solution were added to the reactor under continuous magnetic stirring. Then, appropriate ozone stock solutions were added to the reactor to initiate catalytic ozonation (the initial mixing solution contained 50 µg L⁻¹ atrazine, 20 mg L⁻¹ catalyst and 1 mg L⁻¹ O₃). The solution of an appropriate volume was sampled from the reactor at certain intervals, filtered with a 0.22 µm prefilter and quenched with a trace of Na₂S₂O₃ for further analysis. Two samples were repeated for each experiment.

2.4. Characterization

The XRD patterns were recorded in the 2θ range of 5–60° using a Rigaku Ultima V diffractometer with Cu Kα as the radiation source. The surface area was measured on an automatic adsorption analyzer (ASAP2460, Micromeritics Instrument Corp., Norcross, GA, USA) and calculated by the Brunauer–Emmett–Teller (BET) method. The structure and morphology of the as-prepared CeO₂ were characterized by transmission electron microscopy (FEI Tecnai G2 F20, NL) and scanning electron microscopy (Zeiss Sigma 300, GER) equipped with an energy-dispersive spectrometer. The elementary compositions of the prepared samples were analyzed by X-ray photo-electron spectroscopy (Thermo Fisher Scientific, Waltham, MA, USA).

The atrazine concentration was detected by high-performance liquid chromatography (LC-20AT, Shimadzu, JPN) equipped with a diode array detector. A reversed-phase C18 column was used under isocratic elution with methanol and phosphoric acid solution (*v/v*, 55:45) at 1.0 mL/min at 35 °C. The intermediates were identified by an ultra-performance liquid chromatography tandem quadrupole time of flight mass spectrometer (LCMS-9030, Shimadzu). Gaseous O₃ concentrations were monitored using an ozone analyzer (GM-6000-OEM, ANSEROS). Aqueous O₃ concentrations were measured by iodometry and were calculated using the following equation.

$$C_{(O_3)} = 24000C_{(Na_2S_2O_3)}V_{(Na_2S_2O_3)}/V_{(O_3)} \quad (1)$$

where $C_{(O_3)}$ is the aqueous O₃ concentration, mg/L; $C_{(Na_2S_2O_3)}$ is the concentration of Na₂S₂O₃ standard solution, mol/L; $V_{(Na_2S_2O_3)}$ is the consumed volume of Na₂S₂O₃ standard solution, mL; $V_{(O_3)}$ is the titration volume of the aqueous O₃, mL.

3. Results and Discussion

3.1. Characterization of CeO₂

The XRD patterns of the CeO₂ samples are shown in Figure 1. The synthetic and commercial samples both exhibited five distinguished diffraction peaks at 28°, 33°, 47°, 56° and 59°, which could be indexed to the (111), (200), (220), (311) and (222) reflection planes of CeO₂ (JCPDS No. 78-0694) [22]. The peaks of synthetic CeO₂ were wider and weaker than those of commercial CeO₂, which implied that the crystal size of synthetic CeO₂ was smaller than that of commercial CeO₂. The average crystal size of the synthetic and commercial CeO₂ was 9.8 nm and 37.4 nm, respectively, through the calculation of the Scherrer formula as below [23].

$$D = K\lambda / \beta \cos\theta \quad (2)$$

where D is the average crystal size; K is a constant of 0.89; λ is the X-ray wavelength of 0.154 nm; β is the full width at half maximum of the diffraction peak; θ is the diffraction angle.

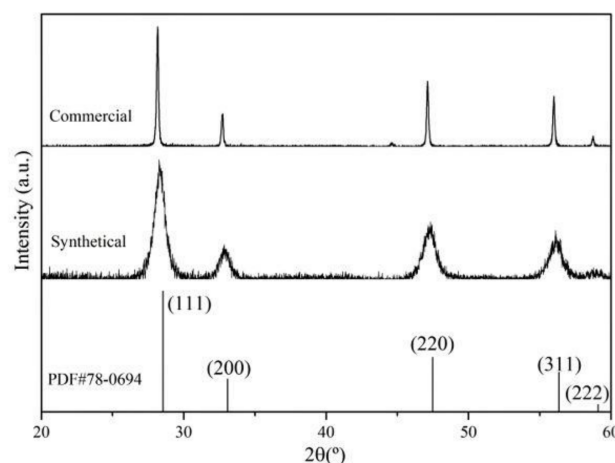


Figure 1. XRD pattern of CeO₂ samples.

The BET adsorption-desorption isotherms were measured to analyze the specific surface area and pore information of CeO₂. In Figure 2a, the hysteresis loop of the synthetic CeO₂ corresponded to type IV, indicating the existence of mesopores. The commercial CeO₂ might be nonporous or microporous since its hysteresis loop belonged to type I. Moreover, the specific surface area of the synthetic and commercial CeO₂ shown in Table S1 was 95.08 m²/g and 1.44 m²/g, respectively, and the specific surface area of the synthetic CeO₂ was significantly higher than that of the commercial CeO₂, which implied that the synthetic CeO₂ would provide more catalytic sites and facilitate catalytic ozonation as it could offer more active site exposure possibilities compared to the commercial CeO₂ of the same mass. Figure 2b showed that the synthetic CeO₂ had a relatively concentrated pore distribution while the commercial CeO₂ was almost non-porous, which echoed the analysis of BET adsorption-desorption isotherms and implied that the synthetic CeO₂ might be of ordered mesopores.

The morphologies of CeO₂ were characterized by SEM, and the images are shown in Figure 3. Apparently, the CeO₂ samples presented different degrees of aggregated morphology, and the synthetic CeO₂ seen in Figure 3a,c exhibited granular while the commercial CeO₂ seen in Figure 3b,d exhibited layered, which implied that the surface area of synthetic CeO₂ would be much higher than that of commercial CeO₂. Figure 4 displays the TEM images of CeO₂ within different nanometer dimensions. Through the comparison of samples, the synthetic CeO₂ exhibited higher dispersibility than the commercial CeO₂, which was consistent with the SEM results. Moreover, the synthetic CeO₂ was a nanorod with well-ordered channels, while the commercial CeO₂ was a nanocube with high agglomeration. Further, the nanorod was 10.16 nm in diameter, and

the distance between each channel was 2.18 nm, implying the synthetic CeO₂ had an ordered mesoporous structure and would have large active sites exposed. The synthetic CeO₂ dominantly exposed (111) facets with an interplanar spacing of 0.31 nm, while the commercial CeO₂ mainly exposed (200) facets with an interplanar spacing of 0.19 nm. The lattice fringes revealed the high crystallinity of CeO₂, which further proved the results of XRD.

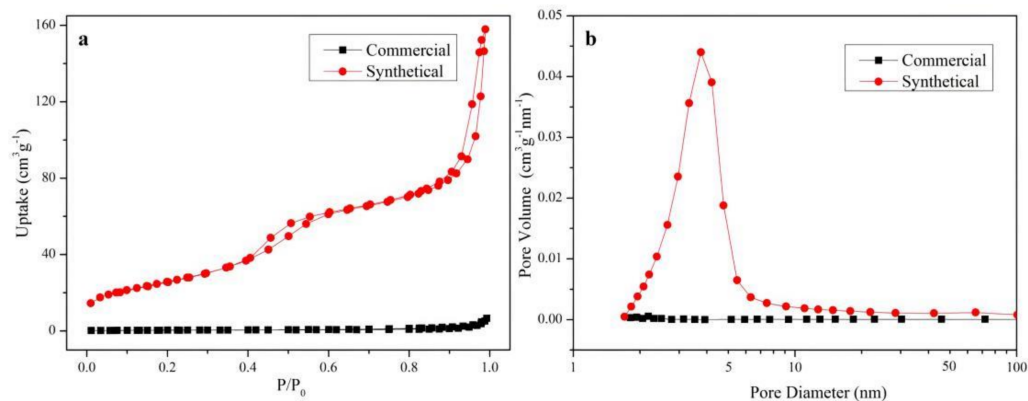


Figure 2. Nitrogen adsorption-desorption isotherms (a) and pore size distribution (b) of CeO₂.

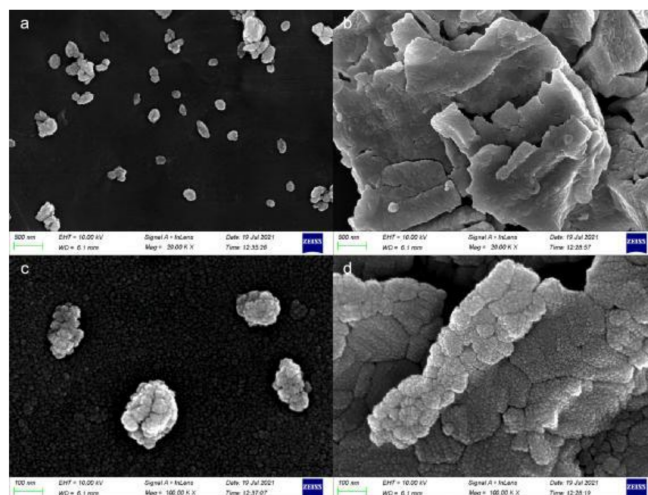


Figure 3. SEM images of synthetic (a,c) and commercial (b,d) CeO₂.

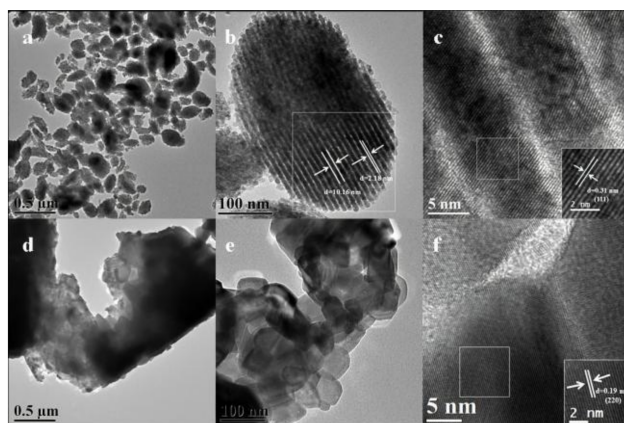


Figure 4. TEM images of synthetic (a–c) and commercial (d–f) CeO₂ within different nanometer dimensions.

The redox couple between $\text{Ce}^{3+}/\text{Ce}^{4+}$ or O^{2-}/O_3 plays a crucial role in enhancing the catalytic activity as the electrons from Ce^{3+} would be transferred to O_3 , which decomposes O_3 into reactive oxygen species, and the electrons from O^{2-} would reduce the Ce^{4+} to Ce^{3+} [21]. The chemical states of Ce/O and their concentrations on the sample surface were analyzed from the XPS spectra. As illustrated in Figure 5a, the Ce 3d XPS spectra consisted of two series of spin-orbit lines, where v represented the Ce 3d_{3/2} spin-orbit splitting peak while u represented the Ce 3d_{5/2} spin-orbit splitting peak. The spin-orbit was well-fitted with ten peaks through deconvolution [24], and the energy positions of these ten spin-orbit components were summarized in Table S2. Taking the synthetic sample as an example, three pairs of peaks, including v (882.46 eV) and u (900.98 eV), v'' (888.87 eV) and u'' (907.61 eV), and v''' (898.18 eV) and u''' (916.83 eV), were related to the characteristic peaks of Ce^{4+} . The remaining two pairs of peaks marked as v₀ (880.38 eV) and u₀ (898.38 eV) and v' (884.84 eV) and u' (903.05 eV) belonged to the characteristic peaks of Ce^{3+} [24]. The results indicated that cerium existed in CeO_2 in two valence states [25], Ce^{3+} and Ce^{4+} , and the atomic ratio of Ce^{3+} to Ce^{4+} was 10.14% and 12.59% for the synthetic and commercial CeO_2 , respectively. The emergence of multivalent cerium would facilitate the charge transfer and the production of reactive oxygen species during the catalytic ozone process. The presence of Ce^{3+} would introduce the occurrence of oxygen vacancies on CeO_2 . As illustrated in Figure 5b, the O 1s XPS spectra exhibited a strong peak with a shoulder, and might be related to four kinds of surface oxygen states. The fitting peak at 529.47–529.51 eV could be attributed to the lattice oxygen [26], the one at 530.51 eV could be assigned as the surface oxygen from the hydroxyl group [27], and the adjacent peaks at 531.46–531.47 eV and 531.81–531.97 eV should be characteristic of subsurface $\text{O}^-/\text{O}_2^{2-}$ species, which belong to oxygen substances chemically adsorbed at oxygen vacancies and would improve the catalytic activity [28].

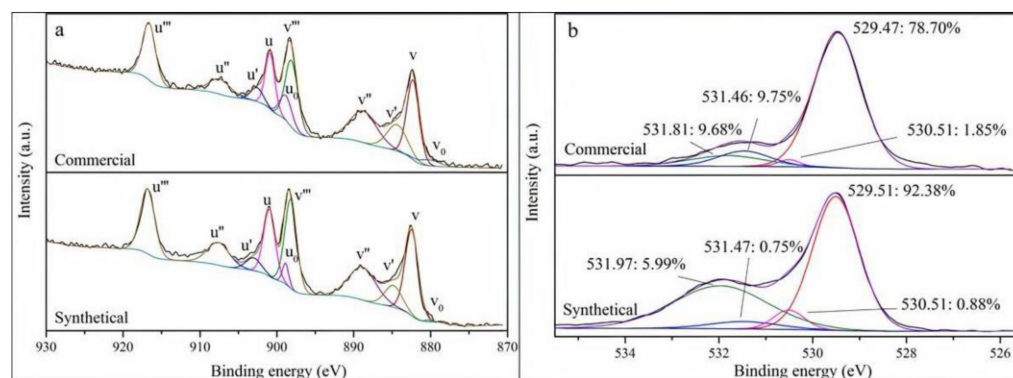


Figure 5. XPS spectra of Ce 3d (a) and O 1s (b) of CeO_2 .

3.2. Catalytic Ozonation of Atrazine

To evaluate the catalytic superiority of the synthetic CeO_2 for ozonation, the atrazine degradation experiments were carried out under different conditions. The adsorption was performed for 10 min before atrazine degradation. As shown in Figure 6a, the adsorption amount of synthetic CeO_2 was as high as 9.9%, while that of the commercial one was only 4.0%. The good adsorption capacity is attributed to the high surface area of synthetic CeO_2 , which would be favorable for the reaction of atrazine with hydroxyl radical generated on the catalyst surface. The atrazine removal rate with synthetic CeO_2 could reach up to 85.5% after 10 min, while the removal rates with commercial CeO_2 and ozone alone were 64.8% and 46.4%, respectively. The performance of synthetic CeO_2 on catalytic ozonation of atrazine was statistically ($p < 0.05$) different from and better than that of commercial CeO_2 or ozone alone, indicating that the synthetic CeO_2 effectively enhanced the catalytic ozonation and its catalytic activity was obviously superior to commercial CeO_2 . The nano-ZnO [29] and mesoporous Fe_3O_4 [30] were also prepared as ozonation

catalysts to enhance the degradation of atrazine, and in contrast, the synthetical CeO₂ could obtain the high removal efficiency of atrazine at a dose of less than an order of magnitude. To further quantitatively analyze the catalytic activity of CeO₂, the rate constants were calculated according to the pseudo-first-order kinetic equation [13]:

$$-\ln(C_t/C_0) = k_{obs}t \quad (3)$$

where C_t is the atrazine concentration at the reaction time t , C_0 is the initial atrazine concentration, and k_{obs} is the pseudo-first-order constant. As shown in Figure 6b, the apparent rate constant for ozone alone was 0.074 min⁻¹, while the apparent rate constant increased to 0.175 min⁻¹ and 0.097 min⁻¹ after the addition of synthetical and commercial CeO₂, which demonstrated that the applied CeO₂ could promote the removal of atrazine. Notably, the apparent rate constant of synthetical CeO₂ was significantly higher than that of commercial CeO₂, which was associated with the superior aforementioned properties such as mesoporous structure, high surface area, as well as good dispersibility.

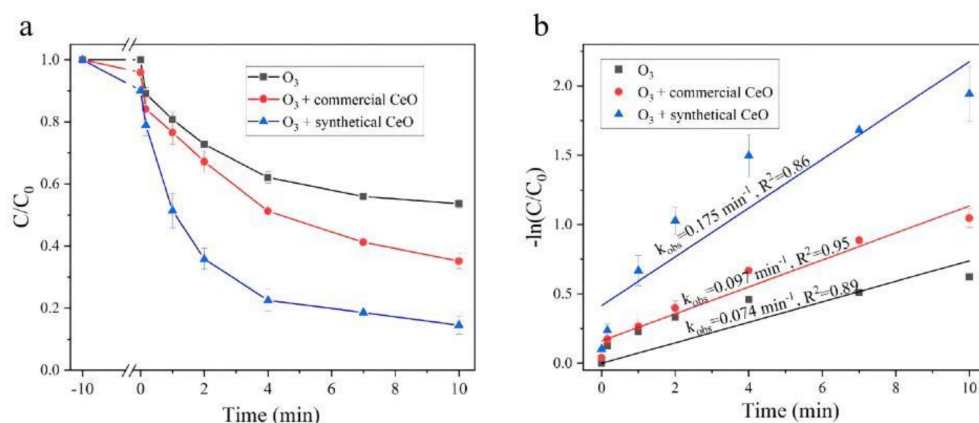
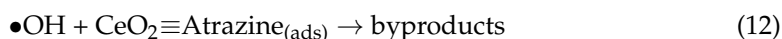
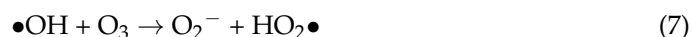
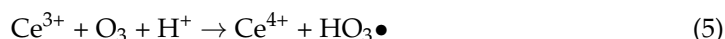


Figure 6. The curves (a) and pseudo-first-order plots (b) of atrazine degradation in different processes (atrazine concentration = 50 µg/L; catalyst dose = 20 mg/L; ozone concentration = 1 mg/L; initial pH = 7).

Combined with the experimental results and previous research [31], the atrazine degradation was a relatively complex process during the catalytic ozonation, which included adsorption, direct oxidation by molecular ozone and indirect oxidation by hydroxyl radical. The catalytic mechanism of synthetical CeO₂ on the ozonation of atrazine could be summarized as follows:



The pH value has an important influence on the chemical characteristics of the catalyst surface, the charge of ionic organic molecules, and the decomposition of O_3 into reactive oxygen species in the catalytic process [32]. The influence of the initial pH value on the catalytic efficiency would be taken into account in the subsequent evaluation of the environmental influence on the catalytic performance.

3.3. Transformation Products and Proposed Pathways

The molecular structure of atrazine mainly consists of the s-triazine ring, the isopropylamino group, the ethylamino group and the chlorine group, and the nitrogen atom in the amino group and the chlorine atom adjacent to the s-triazine ring are vulnerable to radical oxygen species [15]. It is widely recognized that the degradation of atrazine in catalytic ozonation involves the reaction pathways: dealkylation, dechlorination, deamination and olefination [33]. However, the priority of the pathways was basically not involved in previous studies on reaction pathways since the sampling time for the determination of intermediates was not considered.

The previous results shown in Figure 5a indicated that atrazine could be mostly degraded within 10 min, and half could be degraded in one minute. The sample after one minute of catalytic ozonation could better reflect the early reaction process and was used for the determination of intermediates. Eight organic intermediates with m/z values of 232, 174, 214, 230, 172, 212, 188 and 146 were successfully identified (mass error within 0.5 ppm), and were shown in Table S3 and Figure S1. Based on the intermediates and literature reports, the degradation pathway for the catalytic ozonation of atrazine was proposed in Figure 7. Apparently, the structural changes of atrazine first occurred in the isopropylamino and ethylamino groups. Six intermediate products were detected during the change of the ethylamino group, and their mass spectral peak responses were relatively higher, which could be inferred that the change of the ethylamino group was the main pathway of atrazine degradation. The ethylamino group was attacked by hydroxyl radicals to form the hydroxylated intermediate P1($m/z = 232$), and the formed hydroxyl group could be easily attracted to form carbon-centered radicals, which could further add oxygen and rapidly eliminate hydroxyl peroxide radical to generate ketones P4($m/z = 230$) [34], and further attacked by hydroxyl radicals, leading to the loss of chlorine and the formation of hydroxylated intermediate P6($m/z = 212$). The intermediate P3($m/z = 232$) was formed from the olefination of P1, followed by further dealkylation to form the intermediate P5($m/z = 172$) [35]. It is noted that the dealkylation reactions were ubiquitous, and the intermediates P2($m/z = 174$), P5, P7 and P8($m/z = 146$) were the products of dealkylation reactions since the nitrogen atoms on the isopropylamino group and ethylamino group were prone to being attacked, resulting in the heterolytic cleavage of the C–N bond [15]. These intermediates were also observed in other advanced oxidation processes, such as photocatalytic oxidation, persulfate oxidation and Fenton oxidation. All the above intermediates would be further oxidized to low molecular organics and even mineralized to CO_2 and H_2O by prolonging the reaction time, which was widely investigated in previous studies [29]. The results indicated that the initiating reaction of catalytic ozonation of atrazine mainly occurred on the ethylamino group and proceeded to the dealkylation reactions.

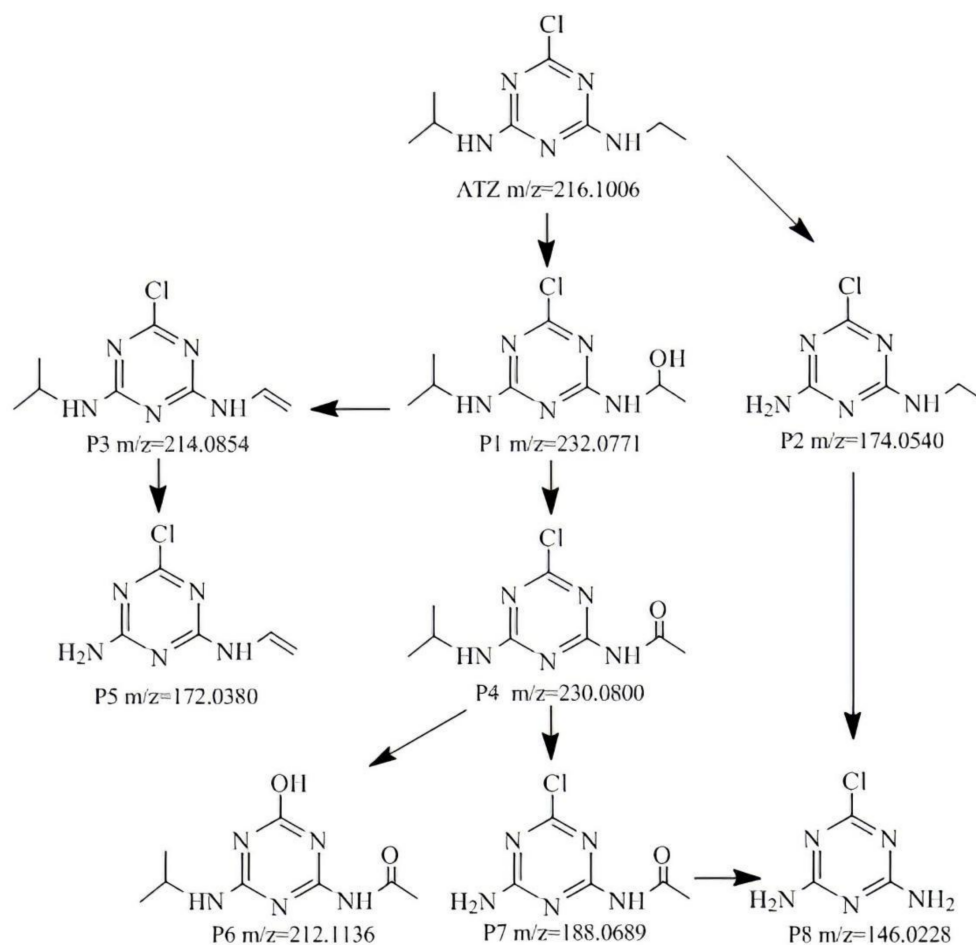


Figure 7. Proposed degradation pathway of atrazine.

4. Conclusions

The mesoporous CeO_2 was successfully obtained by the nanocasting method and investigated for catalytic ozonation of atrazine. Compared with commercial CeO_2 and single ozone, synthetic CeO_2 significantly enhanced the removal of atrazine due to its excellent properties such as high surface area, well-ordered mesoporous structure and redox $\text{Ce}^{3+}/\text{Ce}^{4+}$ couple. Eight organic intermediates were identified, and the initiating reaction of catalytic ozonation of atrazine mainly occurred on the ethylamino group, followed by the dealkylation reactions. This study might facilitate the application of mesoporous metal oxide and the understanding of the degradation pathways of organic pollutants in catalytic ozonation.

Supplementary Materials: The following supporting information can be downloaded at: <https://www.mdpi.com/article/10.3390/w14213431/s1>, Figure S1. HPLC-MS/MS chromatogram of atrazine and intermediates; Table S1. Physical properties of the catalysts; Table S2. Energy positions of Ce spin orbit components in different samples (unit: eV); Table S3. UPLC-MS/MS analysis of atrazine and intermediates. Reference [36] is cited in the supplementary material.

Author Contributions: J.Z.: Methodology, Software, Investigation, Writing—original draft; T.Z.: Writing—review & editing, Supervision, Data curation; S.L.: Investigation, Writing—review & editing; S.S.: Software, Writing—review & editing; Y.W.: Writing—review & editing; X.L.: Writing—review & editing; J.W.: Writing—review & editing; R.L.: Resources, Writing—review & editing. All authors have read and agreed to the published version of the manuscript.

Funding: This research received no external funding.

Data Availability Statement: Not applicable.

Acknowledgments: The authors would like to acknowledge the support for this work by the Beijing Key Laboratory of Aqueous Typical Pollutant Control and Water Quality Safeguard.

Conflicts of Interest: The authors declare no conflict of interest.

References

1. Salazar-Ledesma, M.; Prado, B.; Zamora, O.; Siebe, C. Mobility of atrazine in soils of a wastewater irrigated maize field. *Agric. Ecosyst. Environ.* **2018**, *255*, 73–83. [[CrossRef](#)]
2. Urseler, N.; Bachetti, R.; Biolé, F.; Morgante, V.; Morgante, C. Atrazine pollution in groundwater and raw bovine milk: Water quality, bioaccumulation and human risk assessment. *Sci. Total Environ.* **2022**, *852*, 158498. [[CrossRef](#)] [[PubMed](#)]
3. Wang, F.; Liu, S.-S.; Feng, Z.; Fu, H.; Wang, M.; Wang, P.; Liu, W.; Wang, C.-C. High-efficient peroxymonosulfate activation for rapid atrazine degradation by FeS_x@MoS₂ derived from MIL-88A(Fe). *J. Hazard. Mater.* **2022**, *440*, 129723. [[CrossRef](#)] [[PubMed](#)]
4. Ge, J.; Cong, J.; Sun, Y.; Li, G.; Zhou, Z.; Qian, C.; Liu, F. Determination of Endocrine Disrupting Chemicals in Surface Water and Industrial Wastewater from Beijing, China. *Bull. Environ. Contam. Toxicol.* **2010**, *84*, 401–405. [[CrossRef](#)] [[PubMed](#)]
5. Navarra, W.; Sacco, O.; Daniel, C.; Venditto, V.; Vaiano, V.; Vignati, D.A.L.; Bojic, C.; Libralato, G.; Lofrano, G.; Carotenuto, M. Photocatalytic degradation of atrazine by an N-doped TiO₂/polymer composite: Catalytic efficiency and toxicity evaluation. *J. Environ. Chem. Eng.* **2022**, *10*, 108167. [[CrossRef](#)]
6. Yeom, Y.; Han, J.; Zhang, X.; Shang, C.; Zhang, T.; Li, X.; Duan, X.; Dionysiou, D.D. A review on the degradation efficiency, DBP formation, and toxicity variation in the UV/chlorine treatment of micropollutants. *Chem. Eng. J.* **2021**, *424*, 130053. [[CrossRef](#)]
7. Yang, L.; Jiao, Y.; Xu, X.; Pan, Y.; Su, C.; Duan, X.; Sun, H.; Liu, S.; Wang, S.; Shao, Z. Superstructures with Atomic-Level Arranged Perovskite and Oxide Layers for Advanced Oxidation with an Enhanced Non-Free Radical Pathway. *ACS Sustain. Chem. Eng.* **2022**, *10*, 1899–1909. [[CrossRef](#)]
8. Ahmed, S.; Rasul, M.G.; Sattar, M.A.; Jahirul, M.I. Phenol degradation of waste and stormwater on a flat plate photocatalytic reactor with TiO₂ on glass slide: An experimental and modelling investigation. *J. Water Process Eng.* **2022**, *47*, 102769. [[CrossRef](#)]
9. Xu, X.; Zhong, Y.; Shao, Z. Double Perovskites in Catalysis, Electrocatalysis, and Photo(electro)catalysis. *Trends Chem.* **2019**, *1*, 410–424. [[CrossRef](#)]
10. Rostami, S.; Jafari, S.; Moeini, Z.; Jaskulak, M.; Keshtgar, L.; Badeenezhad, A.; Azhdarpoor, A.; Rostami, M.; Zorena, K.; Dehghani, M. Current methods and technologies for degradation of atrazine in contaminated soil and water: A review. *Environ. Technol. Innov.* **2021**, *24*, 102019. [[CrossRef](#)]
11. Wang, J.; Chen, H. Catalytic ozonation for water and wastewater treatment: Recent advances and perspective. *Sci. Total Environ.* **2020**, *704*, 135249. [[CrossRef](#)]
12. Li, H.; Zhou, B. Degradation of atrazine by catalytic ozonation in the presence of iron scraps: Performance, transformation pathway, and acute toxicity. *J. Environ. Sci. Health B* **2019**, *54*, 432–440. [[CrossRef](#)]
13. Ye, G.; Luo, P.; Zhao, Y.; Qiu, G.; Hu, Y.; Preis, S.; Wei, C. Three-dimensional Co/Ni bimetallic organic frameworks for high-efficient catalytic ozonation of atrazine: Mechanism, effect parameters, and degradation pathways analysis. *Chemosphere* **2020**, *253*, 126767. [[CrossRef](#)]
14. Zeghioud, H.; Nguyen-Tri, P.; Khezami, L.; Amrane, A.; Assadi, A.A. Review on discharge Plasma for water treatment: Mechanism, reactor geometries, active species and combined processes. *J. Water Process Eng.* **2020**, *38*, 101664. [[CrossRef](#)]
15. He, Y.; Wang, L.; Chen, Z.; Huang, X.; Wang, X.; Zhang, X.; Wen, X. Novel catalytic ceramic membranes anchored with MnMe oxide and their catalytic ozonation performance towards atrazine degradation. *J. Membr. Sci.* **2022**, *648*, 120362. [[CrossRef](#)]
16. Von Gunten, U. Ozonation of drinking water: Part I. Oxidation kinetics and product formation. *Water Res.* **2003**, *37*, 1443–1467. [[CrossRef](#)]
17. Bing, J.; Hu, C.; Nie, Y.; Yang, M.; Qu, J. Mechanism of Catalytic Ozonation in Fe₂O₃/Al₂O₃@SBA-15 Aqueous Suspension for Destruction of Ibuprofen. *Environ. Sci. Technol.* **2015**, *49*, 1690–1697. [[CrossRef](#)]
18. Yuan, L.; Shen, J.; Yan, P.; Chen, Z. Interface Mechanisms of Catalytic Ozonation with Amorphous Iron Silicate for Removal of 4-Chloronitrobenzene in Aqueous Solution. *Environ. Sci. Technol.* **2018**, *52*, 1429–1434. [[CrossRef](#)]
19. Zhang, J.; Zhuang, T.; Liu, S.; Zhang, G.C.; Huo, K. Catalytic ozonation of phenol enhanced by mesoporous MnO₂ prepared through nanocasting method with SBA-15 as template. *J. Environ. Chem. Eng.* **2020**, *8*, 103967. [[CrossRef](#)]
20. Matheswaran, M.; Balaji, S.; Chung, S.J.; Moon, I.S. Studies on cerium oxidation in catalytic ozonation process: A novel approach for organic mineralization. *Catal. Commun.* **2007**, *8*, 1497–1501. [[CrossRef](#)]
21. Afzal, S.; Quan, X.; Lu, S. Catalytic performance and an insight into the mechanism of CeO₂ nanocrystals with different exposed facets in catalytic ozonation of p-nitrophenol. *Appl. Catal. B Environ.* **2019**, *248*, 526–537. [[CrossRef](#)]
22. Piumetti, M.; Bensaid, S.; Russo, N.; Fino, D. Nanostructured ceria-based catalysts for soot combustion: Investigations on the surface sensitivity. *Appl. Catal. B Environ.* **2015**, *165*, 742–751. [[CrossRef](#)]
23. Fan, S.; Song, J.; Xia, Y.; Dai, Q. Catalytic ozonation of thymol with a novel CoCe-MMO catalyst: Kinetics and mechanism. *Environ. Technol. Innov.* **2021**, *24*, 101881. [[CrossRef](#)]
24. Zuo, X.; Ma, S.; Wu, Q.; Xiong, J.; He, J.; Ma, C.; Chen, Z. Nanometer CeO₂ doped high silica ZSM-5 heterogeneous catalytic ozonation of sulfamethoxazole in water. *J. Hazard. Mater.* **2021**, *411*, 125072. [[CrossRef](#)] [[PubMed](#)]

25. Gao, Q.; Cui, Y.; Wang, S.; Liu, B.; Liu, C. Enhanced photocatalytic activation of peroxymonosulfate by CeO₂ incorporated ZnCo-layered double hydroxide toward organic pollutants removal. *Sep. Purif. Technol.* **2021**, *263*, 118413. [[CrossRef](#)]
26. Amri, A.; Duan, X.; Yin, C.-Y.; Jiang, Z.-T.; Rahman, M.M.; Pryor, T. Solar absorptance of copper-cobalt oxide thin film coatings with nano-size, grain-like morphology: Optimization and synchrotron radiation XPS studies. *Appl. Surf. Sci.* **2013**, *275*, 127–135. [[CrossRef](#)]
27. Marco, J.F.; Gancedo, J.R.; Gracia, M.; Gautier, J.L.; Ríos, E.; Berry, F.J. Characterization of the Nickel Cobaltite, NiCo₂O₄, Prepared by Several Methods: An XRD, XANES, EXAFS, and XPS Study. *J. Solid State Chem.* **2000**, *153*, 74–81. [[CrossRef](#)]
28. Gao, J.; Tang, L.; Shen, Z.; Dong, Y.; Wang, Z.; Lyu, J.; Li, J.; Yu, H.-Q. Coupling of SiC and CeO₂ nanosheets to enhance solar energy utilization and optimize catalytic ozonation. *Appl. Catal. B Environ.* **2022**, *317*, 121697. [[CrossRef](#)]
29. Yuan, X.; Yan, X.; Xu, H.; Li, D.; Sun, L.; Cao, G.; Xia, D. Enhanced ozonation degradation of atrazine in the presence of nano-ZnO: Performance, kinetics and effects. *J. Environ. Sci.* **2017**, *61*, 3–13. [[CrossRef](#)]
30. Zhu, S.; Dong, B.; Yu, Y.; Bu, L.; Deng, J.; Zhou, S. Heterogeneous catalysis of ozone using ordered mesoporous Fe₃O₄ for degradation of atrazine. *Chem. Eng. J.* **2017**, *328*, 527–535. [[CrossRef](#)]
31. Qu, Z.; Xu, X.; Ren, H.; Sun, T.; Huang, L.; Gao, Z. Effective mineralization of p-nitrophenol in water by heterogeneous catalytic ozonation using Ce-loaded sepiolite catalyst. *J. Environ. Chem. Eng.* **2022**, *10*, 108185. [[CrossRef](#)]
32. Kasprzyk-Hordern, B.; Ziółek, M.; Nawrocki, J. Catalytic ozonation and methods of enhancing molecular ozone reactions in water treatment. *Appl. Catal. B Environ.* **2003**, *46*, 639–669. [[CrossRef](#)]
33. Yang, Y.; Cao, H.; Peng, P.; Bo, H. Degradation and transformation of atrazine under catalyzed ozonation process with TiO₂ as catalyst. *J. Hazard. Mater.* **2014**, *279*, 444–451. [[CrossRef](#)]
34. Chan, K.H.; Chu, W. Model applications and mechanism study on the degradation of atrazine by Fenton's system. *J. Hazard. Mater.* **2005**, *118*, 227–237. [[CrossRef](#)]
35. Wang, D.; Xu, H.; Ma, J.; Lu, X.; Qi, J.; Song, S. Strong promoted catalytic ozonation of atrazine at low temperature using tourmaline as catalyst: Influencing factors, reaction mechanisms and pathways. *Chem. Eng. J.* **2018**, *354*, 113–125. [[CrossRef](#)]
36. Qiu, X.H.; Su, X.Y.; Li, X.J.; Li, N. Preparation of CeO₂ with Different Morphologies and Its Application to Catalytic Ozonation of Aqueous Lemon Yellow Solutions. *Adv. Mater. Res.* **2014**, *997*, 3–8. [[CrossRef](#)]